Structural design of mid-infrared waveguide detectors based on InAs/GaAsSb superlattice

PEI Jin-Di[1]，　CHAI Xu-Liang[1]，　WANG Yu-Peng[1]，　ZHOU Yi[1,2*]

（1. School of Physics and Optoelectronic Engineering, Hangzhou Institute for Advanced Study, University of Chinese Academy of Sciences, Hangzhou 310024, China;
2. Key Laboratory of Infrared Imaging Materials and Detectors, Shanghai Institute of Technical Physics, Chinese Academy of Sciences, Shanghai 200083, China）

Abstract：In the realm of near-infrared spectroscopy, the detection of molecules has been achieved using on-chip waveguides and resonators. In the mid-infrared band, the integration and sensitivity of chemical sensing chips are often constrained by the reliance on off-chip light sources and detectors. In this study, we demonstrate an InAs/GaAsSb superlattice mid-infrared waveguide integrated detector. The GaAsSb waveguide layer and the InAs/GaAsSb superlattice absorbing layer are connected through evanescent coupling, facilitating efficient and high-quality detection of mid-infrared light with minimal loss. We conducted a simulation to analyze the photoelectric characteristics of the device. Additionally, we investigated the factors that affect the integration of the InAs/GaAsSb superlattice photodetector and the GaAsSb waveguide. Optimal thicknesses and lengths for the absorption layer are determined. When the absorption layer has a thickness of 0.3 μm and a length of 50 μm, the noise equivalent power reaches its minimum value, and the quantum efficiency can achieve a value of 68.9%. The utilization of waveguide detectors constructed with III-V materials offers a more convenient means of integrating mid-infrared light sources and achieving photoelectric detection chips.

Key words：InAs/GaAsSb superlattice, waveguide detector, evanescent coupling, GaAsSb waveguide

基于 InAs/GaAsSb 超晶格的中红外波导探测器结构设计

裴金狄[1]，　柴旭良[1]，　王昱彭[1]，　周　易[1,2*]
（1. 国科大杭州高等研究院 物理与光电工程学院，浙江 杭州 310024；
2. 中国科学院上海技术物理研究所 红外成像材料与器件重点实验室，上海 200083）

摘要：在近红外领域，已经利用片上波导和谐振器实现了分子的光谱检测。然而在中红外波段，许多传感器仍使用芯片外光源和探测器，这限制了化学传感芯片的集成度和灵敏度。本文设计了一种 InAs/GaAsSb 超晶格中红外波导集成探测器，采用 GaAsSb 作为中红外波导，波导层和 InAs/GaAsSb 超晶格吸收层之间采用倏逝波耦合方式，可以实现低损耗和高响应度的中红外光探测。对器件的光电特性进行了模拟，着重分析了 InAs/GaAsSb 超晶格光电探测器与 GaAsSb 波导集成的影响因素，得到了吸收区的最优厚度和长度。当吸收区的厚度为 0.3 μm、长度为 50 μm 时，噪声等效功率最低，量子效率可以达到 68.9%。基于 Ⅲ-Ⅴ 族材料的波导探测器更容易集成中红外光源，实现中红外的片上集成光电检测芯片。

关　键　词：InAs/GaAsSb 超晶格；波导探测器；倏逝波耦合；GaAsSb 波导

中图分类号：TN304.2；TN305　　　**文献标识码**：A

Introduction

The mid-infrared band comprises two distinct atmospheric windows of 3-5 μm and 8-14 μm. It includes the thermal radiation features of objects and molecular fingerprint regions. Consequently, the mid-infrared band is extensively across various domains, including infrared thermal imaging[1], biomedical diagnostics[2], and material analysis[3]. Optoelectronic Integrated Circuits (OEIC) encompass the integration of optoelectronic and microelectronic technologies on a single chip, enabling the consolidation of components for various functions such as generation, transmission, modulation, reception, and processing onto a shared substrate. The advancement of mid-infrared optoelectronic integration is of significant research importance due to its potential to enable the development of compact, chip-level sensors. Waveguide detectors play a crucial role in the integration of optoelectronic devices. In the context of waveguide-integrated detectors, the process of optical signal coupling into the absorption layer occurs gradually as the signals propagate within the waveguide. As light propagates through the waveguide, it is concurrently absorbed within the absorption layer. The direction of light propagation is perpendicular to the direction of transport of photo-generated carriers. This particular design can increase bandwidth while maintaining responsivity at its current level[4]. It enables efficient absorption along the entire waveguide, providing a larger absorption area. Consequently, it is feasible to sustain a thin absorption layer while ensuring a high quantum efficiency. This design accelerates the transit of photo-generated carriers across the depletion layer, thereby greatly augmenting the bandwidth of the detector. However, the development of mid-infrared waveguide detectors is faced with challenges arising from the integration of infrared-transparent waveguide materials and narrow-bandgap semiconductor detector materials, thereby adding complexity to the process. Penades, J Soler[5] et al. proposed a silicon slot waveguide on an insulator with a propagation loss of (-1.4±0.2) dB/cm at a wavelength of 3.8 μm. Fangxin Li[6] et al. reported a low-loss silicon sapphire nanowire with a transmission loss of less than -2 dB/cm at 5.18 μm. Barritault P[7] et al. proposed a waveguide platform with a thick epitaxial silicon-based graded SiGe waveguide. This waveguide demonstrates remarkably low waveguide losses, measuring only -1 dB/cm at 4.5 μm. Aldo Gutierrez-Arroyo et al.[8] used the Ge-Sb-Se multilayer structure to make a waveguide, achieving a transmission loss of -2.5 dB/cm at 7.7 μm. Wei Li et al.[9] proposed a GON waveguide that grew Ge on Si_3N_4 and had a waveguide loss of -3.35 dB/cm at 3.8 μm. The current focus of waveguide-integrated detector development is mostly on silicon-based materials and focuses on the visible and near-infrared spectrum, with less attention on mid-infrared research. Notable research efforts have been reported, including M. Muneeb[10] et al.'s integration of PIN photodiodes based on $InAs_{0.91}Sb_{0.09}$ on the SOI platform, achieving a responsivity of 0.3 A/W at 3.8 μm. Zhibo Qu[11] et al. have reported a waveguide-integrated detector utiliz-

ing metal-graphene-metal at 3.8 μm, with a responsivity of 2.2 mA/W. Li Huang[12] et al. proposed a mid-infrared detector scheme integrating black phosphorus on the SOI platform, achieving a responsivity of 23 A/W at 3.68 μm and 2 A/W at 4 μm, with a noise equivalent power of less than 1 nW/$Hz^{1/2}$ at room temperature. Swapnajit Chakravarty[13] et al. achieved high sensitivity gas sensing by integrating quantum cascade detectors within photonic crystal slot waveguides using the InGaAs/InP material system. They successfully detected 3 ppm of carbon monoxide (CO) at 4.55 μm. In a separate study conducted on the SoS platform[14], they detected 10 ppm of the chemical warfare simulant triethyl phosphate (TEP) at 3.4 μm.

The emergence of InAs/GaAsSb type-II superlattice materials introduces a novel technology for infrared detection and offers new possibilities for mid-infrared waveguide detectors[15]. By adjusting the thickness and composition of InAs and GaAsSb layers, it is possible to modify the detection wavelength to cover a wide range from 3 μm to 30 μm. The utilization of lattice-matched GaAsSb as the waveguide layer enables reduced loss within the 3-5 μm spectral range. Growing the waveguide and detector on one chip offers higher integration, eliminating issues associated with device coupling, and aligning with the requirements of OEIC. This study introduces a detector integrated with a mid-infrared waveguide, specifically designed on an InAs substrate. It employs evanescent coupling to effectively direct light into the absorption layer of the InAs/GaAsSb type-II superlattice through the GaAsSb waveguide layer. We presented a simulation of the optical and electrical characteristics of devices. To ensure the accuracy of the computational model, we conducted a comparative analysis with the results of other research teams[17] and found similar approaches, such as simulation of beam propagation and the analysis of quantum efficiency. We conducted an analysis of the factors that influenced the performance of the InAs/GaAsSb superlattice photodetector when integrated with a GaAsSb waveguide.

1 Design and simulation

The optical detection of the waveguide detector was simulated using the finite element method. Figure 1 shows the simulation structure of the waveguide-integrated detector and the simulated propagation of the optical beam. External optical signals are coupled into the $GaAs_{0.09}Sb_{0.91}$ waveguide and subsequently detected by the photodiode following propagation. Due to the comparable refractive index of the absorption layer and the waveguide layer, light can penetrate the waveguide layer and enter the absorption layer. Once light is absorbed, it initiates the generation of electron-hole pairs, with electrons and holes being collected by the n-type and p-type contact layers, respectively. It is assumed that the absorption of each photon leads to the generation of an electron-hole pair, thereby establishing a direct relationship between the absorption rate of the absorption layer and its quantum efficiency. The refractive index of GaAsSb is

3. 75 at 4. 6 μm，allowing for negligible absorption. A heavily doped InAs layer is positioned beneath the GaAsSb waveguide layer，with a refractive index of 3. 1 [18]，in order to effectively inhibit the leakage of light towards the substrate. The absorption coefficient and refractive index of the InAs/GaAs$_{0.09}$Sb$_{0.91}$ （2. 1 nm InAs/2. 1 nm GaAs$_{0.09}$Sb$_{0.91}$） superlattice material are illustrated in Fig. 2.
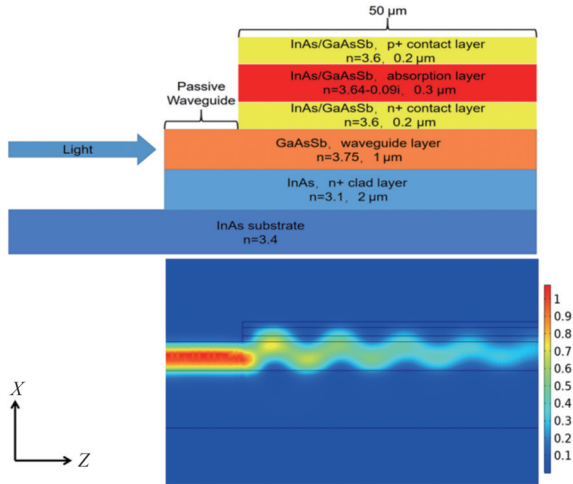

Fig. 1　Schematic structure of the waveguide detector and optical beam propagation simulation
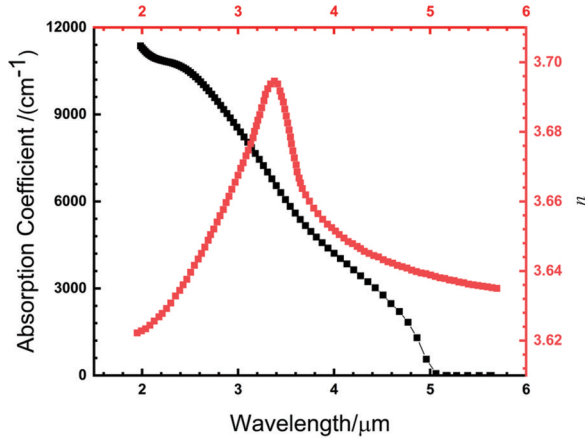图 1　波导集成探测器结构示意图和光束传播模拟

Fig. 2　Absorption coefficient and refractive index of InAs/GaAsSb superlattice
图 2　InAs/GaAsSb 超晶格材料吸收系数和折射率

Devices with different thicknesses and lengths of the absorption layer were simulated，and the quantum efficiency was calculated. From the obtained results，the responsivity of the device，represented as R，can be expressed as：

$$R = \frac{I_p}{P_0} \qquad , \quad (1)$$

where I_p is the average output current，P_0 is the average input power. I_p can be expressed as：

$$I_p = \frac{q\eta\lambda P_0}{hc} \qquad , \quad (2)$$

where q is the electronic charge，η is the quantum efficiency at the wavelength of λ，h is the Planck constant and c is the speed of light in vacuum. By combining Eqs. （1）and（2），it can be concluded that：

$$R = \frac{q\eta\lambda}{hc} \qquad . \quad (3)$$

In the context of free-space detection，it is observed that the signal-to-noise ratio（SNR）exhibits a proportional relationship with the square root of the detector area. In the case of waveguide-integrated detectors，the distribution of the optical signal across the surface of the detector is not uniform as the light propagates through the waveguide towards the detector. In this scenario，the relationship between SNR and the square root of the detector area is no longer valid. Therefore，the noise equivalent power（NEP）is used as a characterization of SNR，replacing detectivity（$D*$）as the evaluation metric for the device [19]. At ambient temperature，the dark current of the device is primarily dominated by the diffusion current. The diffusion current density can be approximated by the following expression [20]：

$$J = qg_{th}L_n \tanh(\frac{d}{L_n})[\exp(\frac{qv}{KT}) - 1] \qquad , \quad (4)$$

where L_n is the diffusion length，as the absorption layer of the waveguide detector is relatively thin，typically $L_n > d$，g_{th} is the thermal generation rate of minority carrier，$g_{th} = \frac{n_0}{\tau}$，$n_0$ is the concentration of minority carrier，τ is the carrier lifetime of minority carrier，V is the working voltage，d is the thickness of the absorption layer，T is the working temperature，and K is the Boltzmann constant. The expression for NEP is：

$$NEP = \frac{\sqrt{\overline{i_n^2}}}{R_I} \qquad , \quad (5)$$

where R_I is the current response，$\overline{i_n^2}$ is the mean square noise current，assuming that only the current generated by the shot noise is considered here，under reverse bias：

$$\overline{i_n^2} = 2qI_0\Delta f \qquad , \quad (6)$$

where I_0 is the dark current，Δf is the bandwidth. Based on the above equation，it can be concluded that [21]：

$$NEP = \frac{hc\sqrt{2Ag_{th}L_n\tanh(\frac{d}{L_n})[\exp(\frac{qv}{KT}) - 1]\Delta f}}{\eta\lambda} , (7)$$

where A is the area of the detector.

2　Results and analysis

2. 1　Analysis of GaAsSb waveguide loss

It′s essential that the waveguide exhibits excellent transmission capabilities for optical interconnects between the detector and other devices. Therefore，it′s desirable for the GaAsSb waveguide layer exposed to air to support single-mode propagation in order to minimize transmission losses. By utilizing Maxwell′s equations and boundary continuity conditions，the characteristic equation for the TE mode can be obtained：
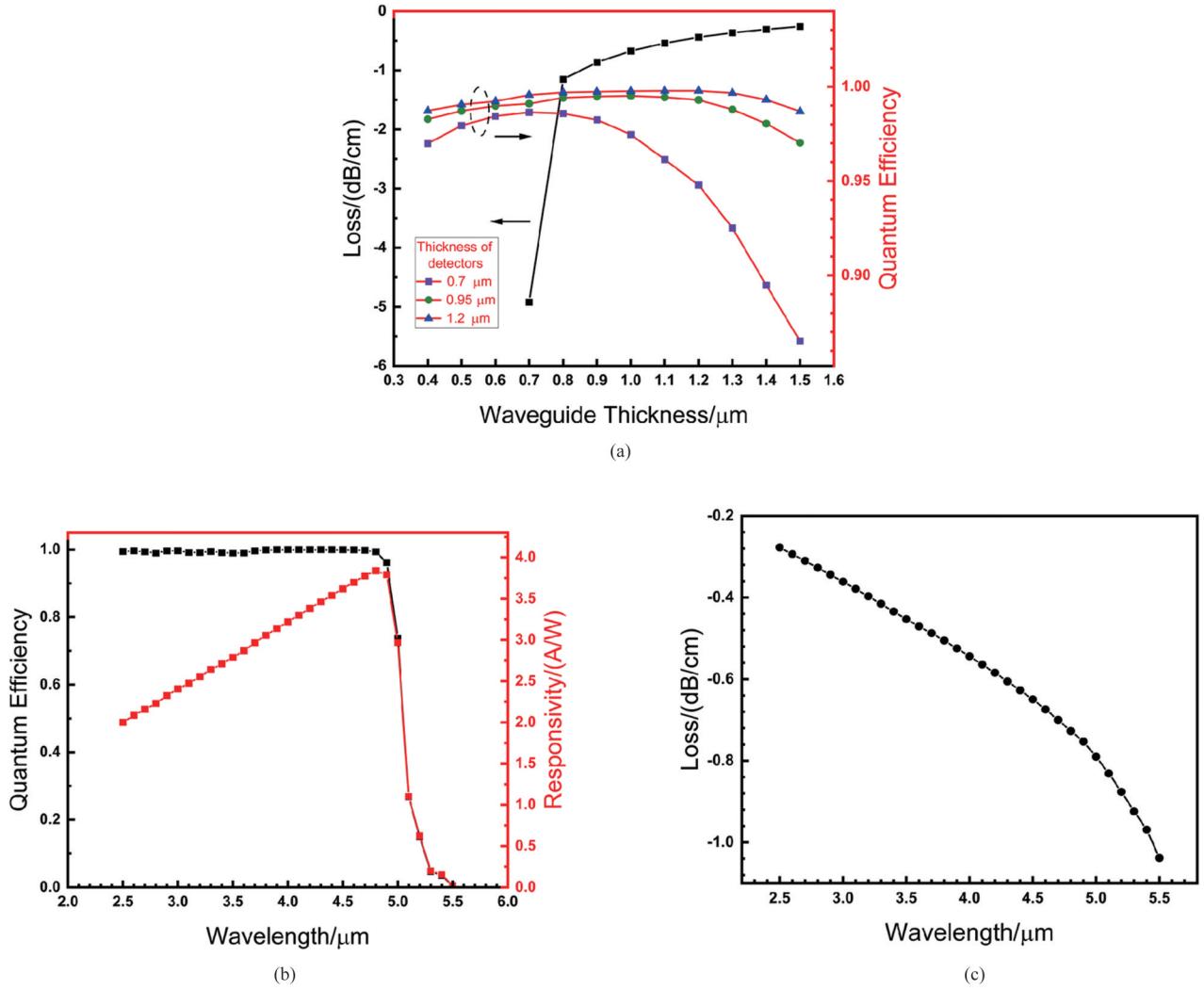
(a)

(b)

(c)

Fig. 3　(a) At a wavelength of 4.6 μm, the variation of waveguide loss with waveguide thickness, and the variation of quantum efficiency with waveguide thickness after the waveguide is integrated with the detector with a length of 200 μm, thicknesses of 0.7 μm, 0.95 μm and 1.2 μm respectively (the thickness here refers to the total thickness of the p-i-n structure, and only the thickness of the absorption layer is different); (b) the variation of quantum efficiency and responsivity of waveguide detector (absorption layer with a length of 200 μm, a thickness of 0.3μm) with wavelength; (c) the relationship between waveguide loss and wavelength

图 3　(a) 工作波长 4.6 μm 下，波导损耗随波导厚度的变化关系，以及波导分别与长 200 μm，厚 0.7 μm、0.95 μm、1.2 μm 的探测器(此处特指 pin 结构的总厚度，且只有吸收层厚度不同)集成后，量子效率随波导厚度的变化关系；(b) 波导探测器(吸收层长 200 μm，厚 0.55 μm)的量子效率和响应度随波长的变化关系；(c) 波导损耗随波长的变化关系

$$\kappa d = m\pi + \arctan\frac{\sqrt{(n_1^2 - n_2^2)K_0^2 - \kappa^2}}{\kappa} +$$
$$\arctan\frac{\sqrt{(n_1^2 - n_3^2)K_0^2 - \kappa^2}}{\kappa} \quad , \quad (8)$$

where κ is the phase constant of GaAsSb waveguide layer in the x-direction, d is the thickness of GaAsSb layer, n_1, n_2, n_3 are the refractive indices of GaAsSb waveguide layer, the doped InAs lower cladding layer and air. K_0 is the wave number in vacuum. The value range of m is an integer starting from 0, representing the order of the mode. When 0. 38 μm < d < 1. 57 μm, the fundamental mode exists and the first-order mode is cut off.

As shown in Fig. 3(a), it can be observed that for waveguide thicknesses below 0. 9 μm, the waveguide loss exceeds -1 dB/cm. This is attributed to insufficient confinement of light by the waveguide layer. The refractive indices of the waveguide and the integrated detector are comparable. When the thickness of the waveguide is comparable to the detector, it satisfies the phase-matching condition for mode coupling. As a result, light can be coupled from the lower waveguide to the upper absorption zone with minimal loss, resulting in a high quantum efficiency. Therefore, both the issue of loss and detector performance should be considered in the selection of waveguide thickness. When the thickness of waveguide layer is 1 μm, the waveguide satisfies the conditions for single-mode transmission, resulting in lower transmission losses （~ -0. 67 dB/cm）. Although the current quantum efficiency is not at its maximum, it still exceeds 97%. We have selected a waveguide with a thickness of 1 μm for the subsequent design. Figure 3(b) illustrates
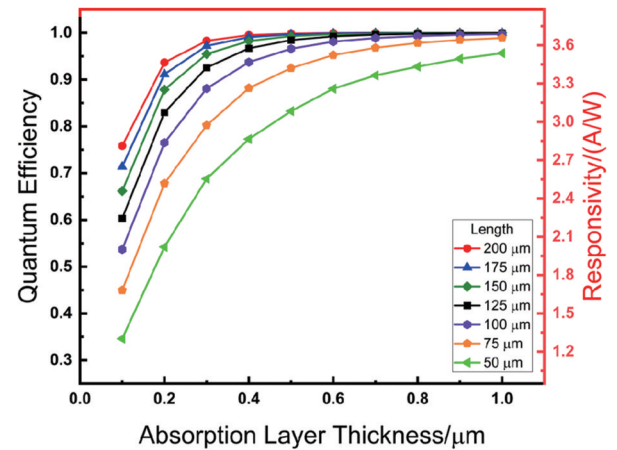
an absorption layer waveguide detector with a length of 200 μm and a thickness of 0.55 μm. It shows the variation of quantum efficiency and responsivity with wavelength. The operational range of the detector is below 5 μm, owing to the influence of InAs/GaAsSb superlattice material. Figure 3（c）shows the loss of the waveguide with wavelength. The waveguide loss is 0.36 dB/cm at 3 μm. As the wavelength increases, there is a decrease in the effective refractive index of the waveguide, resulting in a reduction in the confinement of light and an increase in the distribution of evanescent fields outside the waveguide. This results in greater energy loss, with a waveguide loss of 0.79 dB/cm at a wavelength of 5 μm. Overall, the working wavelength and loss characteristics of the 1 μm-thick GaAsSb waveguide align well with the specified requirements for waveguide detectors.
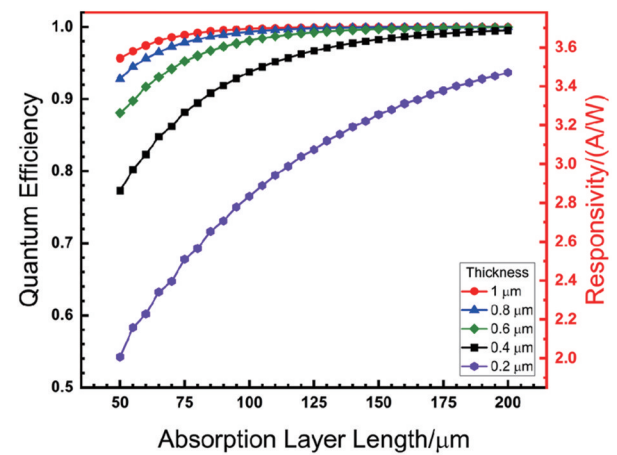
2.2 Waveguide detectors

The performance of waveguide detectors is influenced by the thickness and length of the absorption layer. Figures 4（a）and 4（b）show the variations in quantum efficiency and responsivity, respectively, as a function of the thickness and length of the absorption layer at 4.6 μm. The responsivity exhibits a positive correlation with both the thickness and length of the absorption layer. Even when the absorption layer is of minimal thickness, it is still possible to achieve a quantum efficiency close to 100% by ensuring an adequate length. The maximum current response exhibits a value of 3.7 A/W at 4.6 μm.

Figures 5(a) and 5(b) represent the variation of NEP with absorption layer thickness and length at 4.6 μm. Combining the information from Fig. 4 and Fig. 5, when the quantum efficiency is less than 70%, increasing the length and thickness of the absorption layer results in a reduction in NEP. However, when the quantum efficiency exceeds 70%, further increases in length or thickness lead to a higher quantum efficiency that has a less impact on NEP compared to the increase in dark current, causing NEP to increase.

We found that a waveguide detector with an absorption layer length of 50 μm and a thickness of 0.3 μm has the lowest NEP at 0.39, with 68.9% quantum efficiency and 2.55 A/W responsivity. The methodology for calculating the propagation of optical power along the waveguide and its coupling into the integrated detector is shown in Fig. 6. Optical power absorption predominantly takes place within a relatively short distance. After traversing a distance of 30 μm through an absorbing medium, the optical power decreases by 50%. After a distance of 50 μm, there is a decrease of 70%, and after a distance of 125 μm, there is a decrease of 90%. The light coupling efficiency from the waveguide into the integrated component exceeds 99.9%. There is minimal loss observed during the propagation of light within the waveguide, as it is absorbed by the absorption layer. As the thickness of the absorption layer increases, there is an observed increase in both the dark current and the transit time of carriers. Consequently, this results in a reduction in the bandwidth of the detector. Combined with the

(a)

(b)

Fig. 4   The variation of quantum efficiency and responsivity with the (a) thickness and (b) length of the absorption layer at 4.6 μm

图 4   工作波长 4.6 μm 下,量子效率和响应度随吸收层 (a) 厚度和(b) 长度的变化

analysis of NEP, the impact of absorption layer length on dark current is much smaller than thickness, and it does not have a significant inhibitory effect on the bandwidth. To simultaneously achieve high responsivity, low dark current, and high bandwidth, it is advisable to increase the length of the detector. Therefore, waveguide detectors generally necessitate absorption layers that are thinner and longer. To achieve a high quantum efficiency, it is necessary to decrease the thickness of the waveguide in order to enhance the coupling efficiency between the waveguide layer and the absorption layer. However, this will inevitably lead to increased transmission losses. Therefore, in forthcoming investigations, there is a plan to develop waveguides with varying thicknesses for transmission and coupling. Additionally, tapered couplers will be implemented at the connections to decrease transmission losses and enhance coupling efficiency.
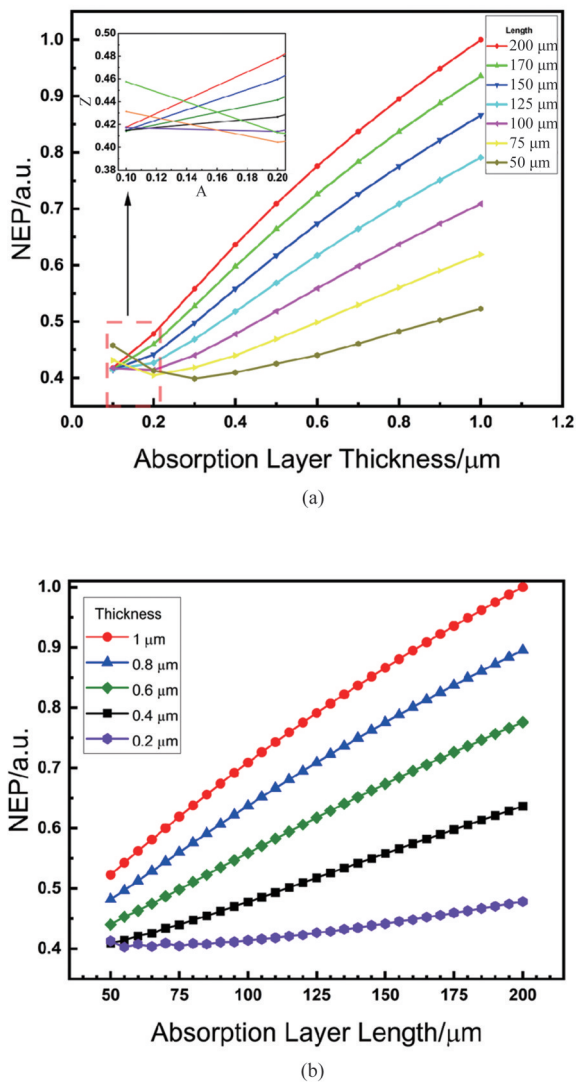
(a)

(b)

Fig. 5 The variation of NEP with the (a) thickness and (b) length of the absorption layer at 4.6 μm

图 5 工作波长 4.6 μm 下，噪声等效功率随吸收层 (a) 厚度和 (b) 长度的变化

3 Conclusion

This paper introduces a novel design for a mid-infrared waveguide utilizing heavily doped InAs and $GaAs_{0.09}Sb_{0.91}$ materials. The transmission loss within the wavelength range of 3-5 μm is consistently below -1 dB/cm, with a loss of -0.67 dB/cm at 4.6 μm. This waveguide not only matches the current mainstream silicon-based waveguide in terms of performance, but also offers the advantage of easier integration with high-performance III-V group semiconductor detectors. Based on the waveguide provided, an integrated $InAs/GaAs_{0.09}Sb_{0.91}$ type-II superlattice detector is implemented, with an absorption layer length of 50 μm and a thickness of 0.3 μm. At 4.6 μm, the quantum efficiency is 68.9%, the responsivity is 2.55 A/W, and NEP is 0.39. With the new type-II superlattice material and long absorption distance, a significant enhancement in quantum efficiency
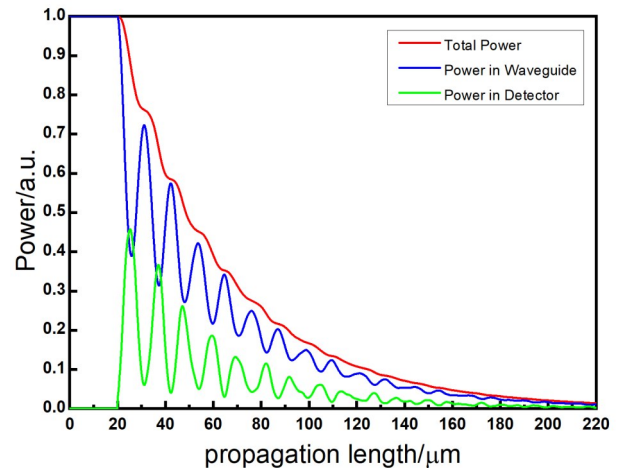

Fig. 6 The variation of power with propagation length in waveguide detector (absorption layer with a length of 200 μm, a thickness of 0.3 μm) after 20 μm propagation in the waveguide

图 6 光沿波导传播 20 μm 后耦合到的波导探测器(吸收层长 200 μm 、厚 0.3 μm)内,功率随传播长度的变化

has been achieved, resulting in a response rate more than twice that of most currently available mid-infrared detectors. At the same time, it has been observed that the dark current diminishes as the cascade order of the absorption region increases. Consequently, the NEP of the detector in question is smaller compared to that of conventional mid-infrared detectors. We conducted simulations to evaluate the impact of structural parameters of the absorption layer on quantum efficiency. Mathematical modeling was subsequently utilized to calculate the responsivity, dark current, and NEP of the integrated device. An analysis of the impacts of various structural parameters is provided. The simulations presented in this study propose a novel concept for mid-infrared waveguide-integrated detectors. The findings provide reference data and theoretical foundations for subsequent experimental designs.

References

[1] Hu J, Meyer J, Richardson K, et al. Feature issue introduction: mid-IR photonic materials [J]. Optical Materials Express, 2013, 3 (9): 1571-1575.

[2] A. M K, Al A G. Advanced Waveguide Based LOC Biosensors: A Minireview [J]. Sensors, 2022, 22(14): 5443-5443.

[3] Min K Y, Jason M, Ali R, et al. InGaAs Membrane Waveguide: A Promising Platform for Monolithic Integrated Mid-Infrared Optical Gas Sensor [J]. ACS sensors, 2020, 5(3): 861-869.

[4] Cui Rong, Yang Xiaohong, Lu Qianqian, et al. Integration of the SOI waveguide with the InGaAs / InP photodetector [J]. Progress in Laser and Optoelectronics, 2014, 51(11): 24-33.(崔荣，杨晓红，吕倩倩，等. SOI波导与InGaAs/InP光电探测器的集成[J]. 激光与光电子学进展), 2014, 51(11): 24-33.

[5] Penades, Soler J, Khokhar, et al. Low-Loss Mid-Infrared SOI Slot Waveguides [J]. IEEE Photonics Technology Letters, 2015, 27(11): 1197-1199.

[6] Fangxin L, D S J, Christian G, et al. Low propagation loss silicon-on-sapphire waveguides for the mid-infrared [J]. Optics express, 2011, 19(16): 15212-15220.

[7] Barritault P, Brun M, Labeye P, et al. Design, fabrication and characterization of an AWG at 4.5 μm [J]. Optics Express, 2015, 23 (20): 26168-26181.

[8] GUTIERREZ-ARROYO A, BAUDET E, BODIOU L, et al. Optical

characterization at 7.7 μm of an integrated platform based on chalco-genide waveguides for sensing applications in the mid-infrared［J］. *Optics Express*，2016，**24**（20）：23109-23117.

［9］Liu J，Sun X，Camacho-Aguilera R，*et al*. Ge-on-Si laser operating at room temperature［J］. *Optics Letters*，2010，**35**（5）：679-681.

［10］M M，A V，A R，et al. III-V-on-silicon integrated micro - spectrometer for the 3 μm wavelength range［J］. *Optics express*，2016，**24**（9）：9465-72.

［11］Qu Z，Nedeljkovic M，Jordi Soler-Penadés，*et al*. Waveguide integrated graphene mid-infrared photodetector［C］. Silicon Photonics XII，2018，105371N-1-105371N-5.

［12］Huang L，Dong B，Guo X，*et al*. Waveguide-integrated blackphosphorus photodetector for mid-infrared applications［J］. *ACS Nano*，2019，**13**（1）：913-921.

［13］Chakravarty S，Midkiff J，Yoo K，*et al*. Monolithic integration of quantum cascade laser，quantum cascade detector，and subwavelength waveguides for mid-infrared integrated gas sensing［C］. Quantum Sensing and Nano Electronics and Photonics XVI，2019，109261V.1-109261V.8.

［14］Rostamian A，Chung C J，Nguyen D，*et al*. Parts-Per-Billion Carbon Monoxide Sensing in Silicon-on-Sapphire Mid-Infrared Photonic Crystal Waveguides［C］. Conference on Lasers and Electro-Optics，2018，1-2.

［15］Xuliang C. Research on the intermediate-wave interband cascade infrared detector［D］. The University of the Chinese Academy of Sciences，2023.（柴旭良 . 中波带间级联红外探测器研究［D］. 中国科学院大学），2023.

［16］Dongdong Y，Tingting H，Qin H，*et al*. High-responsivity 40 Gbit/s InGaAs/InP PIN photodetectors integrated on silicon-on-insulator waveguide circuits［J］. *Journal of Semiconductors*，2016，**37**（11）：54-59.

［17］Zhao Y，Tu J，Li Q，*et al*. Monolithic Integrated InGaAs/InAlAs WDM-APDs With Partially Depleted Absorption Region and Evanescently Coupled Waveguide Structure［J］. *Journal of Lightwave Technology*，2020，**38**（16）：4385-4396.

［18］Paskov，P. P. Refractive indices of InSb，InAs，GaSb，$InAs_xSb1_{-x}$，and $In_{1-x}Ga_xSb$：Effects of free carriers［J］. *Journal of Applied Physics*，1997，**81**（4）：1890-1898.

［19］Lin Hongtao，Sun Boshu，Ma Hui，*et al*. Overview of integrated optoelectronics on mid-infrared film（invited）［J］. Infrared and Laser Engineering，2022，51（01）：155-168.（林宏焘，孙博姝，马辉，等. 中红外片上集成光电子综述（特邀）［J］. **红外与激光工程**），2022，**51**（01）：155-168.

［20］Rui Q Yang. Signal，noises，and detectivities in multi-stage infrared photodetectors［C］. Proc. SPIE 12430，Quantum Sensing and Nano Electronics and Photonics XIX，**124300**E（15 March 2023）. 124300E-1-124300E-10.

［21］Hinkey T R，Yang Q R. Theory of multiple-stage interband photovoltaic devices and ultimate performance limit comparison of multiple-stage and single-stage interband infrared detectors［J］. *Journal of Applied Physics*，2013，**114**（10）：104506.